Notable highlights on locking-free techniques of Reissner-Mindlin plate finite elements in elastostatics

Cong-Uy Nguyen[*1,2], Jean-Louis Batoz[1a] and Adnan Ibrahimbegovic[1b]

[1]*Centre de Recherche Royallieu, Université de Technologie de Compiègne/ Alliance Sorbonne Université, 60200 Compiègne, France*
[2]*Institut für Wissenschaftliches Rechnen, Technische Universität Braunschweig, 38106 Braunschweig, Germany*

Abstract. In this paper, we discuss about the notable locking-free techniques of several simple plate bending finite elements for the Reissner-Mindlin plate bending theory. The brief background for Reissner-Mindlin plate theory is presented, in which stress and strain derivation are given along with one-field and two-field variational approaches. Afterwards, we classify several efficient robust techniques in a cluster of main categories to present sequentially, which are all able to overcome the locking phenomenon in thick plate bending problems. Only selective algorithms are programmed to conduct numerical simulations. The corresponding results are compared between these elements to show their performances.

Keywords: Reissner-Mindlin plate theory; locking-free techniques; simple and efficient algorithms

1. Introduction

Over the course of time, the finite element method has been developed enormously such that many tedious physic problems including solid, fluid, heat mechanics are now possible to be solved by numerical simulation. The geometry and corresponding physical properties of a given problem help the user to select the most appropriate finite element to be used for the simulation. We can count briefly some of the most common finite elements, which have been successfully employed in commercial programs, namely truss, beam, plane stress/strain plate, plate bending, shell, brick or tetrahedron, and even more, see Zienkiewicz *et al.* (2005), Ibrahimbegovic (2009) and Bathe (2016). Regarding the plate bending problem, there are many available techniques and algorithms, which are circulated in the environment of both research and engineering practices. To the rest of this paper, we pay our concentration on the development of several plate bending finite elements, which is challenging topic at the early time and also now in the domain of the finite element method.

One of the pioneering works into the plate bending problem is credited by Mindlin (1951), Reissner (1945) and Reissner (1976), which build the fundamental theory for the thick or lately

---

*Corresponding author, Ph.D. Student, E-mail: cong-uy.nguyen@utc.fr
[a]Professor, E-mail: jean-louis.batoz@utc.fr
[b]Professor, E-mail: adnan.ibrahimbegovic@utc.fr

named as Reissner-Mindlin plate. During that time, there are several efforts in the numerical approach including finite element method for bending thin plate problem or famously named as Kirchhoff-Love plate, see Bazeley *et al.* (1966), Clough and Felippa (1968), Morley (1971) and Hughes *et al.* (1977). One of the main difficulties in solving the Kirchhoff-Love plate is to maintain the continuity of rotation field or so-called C^1 continuity. Based on this property, those finite elements for thin plate problem are classified into two groups including conforming (with C^1 continuity) and non-conforming (without C^1 continuity), see Batoz *et al.* (1980), Batoz (1982) and Ortiz and Morris (1988). One can maintain the C^1 continuity is using the penalty method, which can be found in the works of Cirak and Ortiz (2001) and Viebahn *et al.* (2017). Meanwhile, the numerical method for Reissner-Mindlin plate does not encounter the same problem as in the former since the shear strains are included in the weak form, see Robinson and Haggenmacher (1979), Hughes and Tezduyar (1981), Tessler and Hughes (1983) and Huang and Hinton (1984). Many research efforts produce a number of algorithms for plate bending problem at that time, for a thorough review see Hrabok and Hrudey (1984). Additionally, the recent review on hybrid-mixed low-order finite shell elements can also be found at Lavrencic and Brank (2021). A general overview and clarified details of many developed plate bending and shell problems can be found at Zienkiewicz *et al.* (2005), Batoz and Dhatt (1990) and Batoz and Dhatt (1992). Notably, with the aim to solve the problem better, some of the efficient algorithms are proposed by Batoz and Katili (1992), Ibrahimbegovic (1992), Ibrahimbegovic (1993), Katili (1993), Auricchio and Taylor (1994), Auricchio and Taylor (1994) and Gruttmann and Wagner (2004).

In the modern engineering practices, there are more relevant problems evolving from plate bending problem such as the topic of metal forming, see Guo *et al.* (2000) and the topic of controlling of the plates, see Macchelli *et al.* (2005), Brugnoli *et al.* (2019) and Brugnoli *et al.* (2019). The laminated and composite plates are also the challenging and evolving topics, see Konno and Stenberg (2010), Moleiro *et al.* (2009) and Allaire and Delgado (2016). Similarly, the topological optimization for plates are also branching from the original work of plate bending problem, see Moleiro *et al* (2009), Belblidia *et al.* (2001) and Goo *et al.* (2016). And the fracture computation for plate bending problem can be found at Kiendl *et al.* (2016), Ulmer *et a.l* (2012) and Dolbow *et al.* (2000). As a review paper for notable locking-free algorithms in the plate bending problem, we limit our self in reviewing several simple and efficient numerical algorithms, particularly by finite element method, for the Reissner-Mindlin plate theory. The main focus is in Section 3, the assumed shear strain method can be found in Ibrahimbegovic (1993), Katili (1993), Batoz and Katili (1992) and Katili *et al.* (2014). Another approach is proposed by include shear forces as unknown field, which is added as bubble mode, can be found at Auricchio and Taylor (1994). Batoz (1982) uses the higher-order polynomial to approximate the lateral rotation field to enhance the accuracy. And the final algorithm to be reviewed is the one for quadrilateral plate element, in which it is stabilized and only one integration point is employed in this algorithm, see Gruttmann and Wagner (2004).

The structure of this paper is outlined as follows. In Section 2, the fundamental concepts including the definition of stress, curvature, shear strain and force resultants are given. We illustrate a displacement-based variational principle as well as mixed variational approach, in which other fields such as moment and shear force can also be included in the weak form as independent fields. In Section 3, we present some efficient techniques to overcome the locking phenomenon and produce an accurate solutions for the thick plate bending problem. In Section 4, correspondingly, only three finite elements of the above algorithms are programmed in FORTRAN language. The results from selective simulations are compared between these elements and the built-in FEAP plate element, see Auricchio and Taylor (1994). In Section 5, the conclusions are stated.
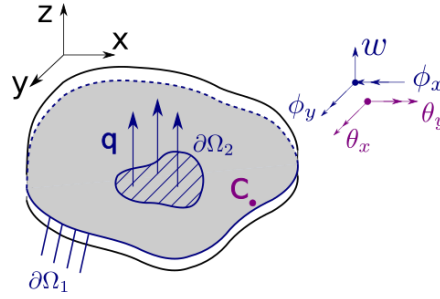
Fig. 1 Plate and sign convention

2. Theoretical background

The brief review on Reissner-Mindlin or so-called thick plate bending theory is discussed in the following section. It is well-known that the Kirchhoff-Love plate theory can be recovered by suppressing the shear fields from the corresponding Reissner-Mindlin plate theory. Subsequently, we present the practical variational approaches including the one-field and multi-field variational principles. The former considers only displacement as independent field, while the latter collaborates on other fields such as moment and shear forces.

2.1 Fundamental concepts

Let Ω be a bounded flat body in R^3 representing a plate of thickness t, see Eq. (1a), in which the thickness t is small compared to the other two dimensions. The corresponding piece-wise smooth boundary $\partial\Omega$, including displacement boundary $\partial\Omega_1$ and stress boundary $\partial\Omega_2$, satisfies Eq. (1b)

$$\Omega = \left\{ (x, y, z) \in \mathbb{R}^3 \,|\, z \in \left[-\frac{t}{2}, +\frac{t}{2} \right], (x, y) \in \mathbb{R}^2 \right\}$$

$$\partial\Omega = \partial\Omega_1 \cup \partial\Omega_2 \quad \text{and} \quad \partial\Omega_1 \cap \partial\Omega_2 = \emptyset$$

(1)

The *xy* plane is placed on the mid-surface and the loading $q(x, y)$ is considered normal to the mid-surface, as shown in Fig. 1. The Reissner-Mindlin plate theory assumes that a straight fiber normal to the mid-surface before loading remains straight but not necessarily normal to the deformed mid-surface. The corresponding rotation components of this fiber are ϕ_x and ϕ_y. The strong governing equations are written following closely the work of Hughes and Brezzi (1989). Both stress and displacement fields are considered as independent fields. The key point here is that the stress is not assumed to be symmetric, but the symmetry of stress tensor is enforced through corresponding moment equilibrium equation of the strong form of the problem $\forall \mathbf{x} \in \Omega$

$$\operatorname{div} \boldsymbol{\sigma} + \mathbf{f} = \rho \ddot{u} \qquad (1)$$

$$\operatorname{skew} \sigma = 0 \qquad (2)$$

$$\operatorname{symm} \boldsymbol{\sigma} = \mathbb{C} \operatorname{symm} \nabla \mathbf{u} \qquad (3)$$

$$u = \bar{u}|_{\partial\Omega_u} \quad \text{and} \quad \sigma n = \bar{t}|_{\partial\Omega_t} \quad (4)$$

(2)

where (1) to (4) are, respectively, the equilibrium equations, the symmetry conditions for stress, the

constitutive equations and the boundary condition. A point P (see Fig. 1), outside of the mid- surface, has displacement components u_x, u_y, u_z. This displacement field can be expressed in terms of lateral defection w at plate mid-surface and fiber rotation vector $\phi(\phi_x, \phi_y)$ which can be written as follows

$$u_x = -z\phi_x(x,y), \quad u_y = -z\phi_y(x,y), \quad u_z = w(x,y) \tag{3}$$

The sign convention of rotation vector $\boldsymbol{\theta}(\theta_x, \theta_y)$ about the *x* and *y* directions is shown in Fig. 1, hence the transformation matrix between rotation vectors $\phi(\cdot)$ and $\boldsymbol{\theta}(\cdot)$ is given as follows

$$\phi_x = -\theta_y \quad \phi_y = \theta_x \tag{4}$$

The displacement field $\mathbf{u}(u_x, u_y, u_z)$ is now interpreted as functions of three selected independent fields

$$u_x = -z\theta_y(x,y), \quad u_y = z\theta_x(x,y), \quad u_z = w(x,y) \tag{5}$$

The corresponding curvature $\boldsymbol{\kappa}$ and shear strain $\boldsymbol{\gamma}$, which are work-conjugates to moment and shear force respectively, can be expressed as follows

$$
\begin{aligned}
\boldsymbol{\kappa} &= \begin{bmatrix} \kappa_x, & \kappa_y, & 2\kappa_{xy} \end{bmatrix}^T &= \begin{bmatrix} \theta_{y,x}, & -\theta_{x,y}, & -\theta_{x,x} + \theta_{y,y} \end{bmatrix}^T \\
\boldsymbol{\gamma} &= \begin{bmatrix} \gamma_{xz}, & \gamma_{yz} \end{bmatrix}^T &= \begin{bmatrix} w_{,x} + \theta_y, & w_{,y} - \theta_x \end{bmatrix}^T
\end{aligned}
\tag{6}
$$

The internal forces include moment $\mathbf{M}$ and shear forces $\mathbf{Q}$, which are defined by integrating of the non-zero stresses through the thickness of the plate, with the notable assumption $\sigma_z=0$

$$
\begin{aligned}
\boldsymbol{M} &= [M_x, M_y, M_{xy}]^T &= \left[\int_{-t/2}^{t/2} \sigma_x z\mathrm{d}z, \int_{-t/2}^{t/2} \sigma_y z\mathrm{d}z, \int_{-t/2}^{t/2} \sigma_{xy} z\mathrm{d}z \right]^T \\
\boldsymbol{Q} &= [Q_x, Q_y]^T &= \left[\int_{-t/2}^{t/2} \sigma_{xz}\mathrm{d}z, \int_{-t/2}^{t/2} \sigma_{yz}\mathrm{d}z \right]^T
\end{aligned}
\tag{7}
$$

The constitutive relations in the case of isotropic linear elastic material are given as follows

$$\boldsymbol{M} = \boldsymbol{C}^b\boldsymbol{\kappa} \quad \text{and} \quad \boldsymbol{Q} = \boldsymbol{C}^s\boldsymbol{\gamma} \tag{8}$$

The corresponding constitutive matrix for moment and shear forces are given explicitly as follows

$$\boldsymbol{C}^b = D \begin{bmatrix} 1 & v & 0 \\ v & 1 & 0 \\ 0 & 0 & (1-v)/2 \end{bmatrix} \quad \text{and} \quad \boldsymbol{C}^s = kGt \begin{bmatrix} 1 & 0 \\ 0 & 1 \end{bmatrix} \tag{9}$$

where the flexural rigidity of plate is $D = \dfrac{Et^3}{12(1-v^2)}$ with E the Young's modulus and v the Poisson's ratio. And $G = \dfrac{E}{2(1+v)}$ is shear modulus and k is the factor accounts for the parabolic variation of transverse shear stress in z-direction. The usual value of k for a homogeneous plate is $k=5/6$.

2.2 One-field variational approach

For the discrete Kirchhof triangle and discrete Kirchhof quadrilateral elements, the formulation is based on the discretization of the strain energy without elaboration on the transverse shear strain energy, see Batoz (1982)

$$U = \frac{1}{2} \int_A \langle \boldsymbol{\chi} \rangle \left[\boldsymbol{D}_b \right] \{ \boldsymbol{\chi} \} \mathrm{d}V \tag{10}$$

in which $\langle \boldsymbol{\chi} \rangle$ is the curvature matrix. Meanwhile, the Reissner-Mindlin plate, the total energy can be written as follows, see Ibrahimbegovic (1993)

$$\Pi(\boldsymbol{u}) = \frac{1}{2} \int_{\Omega} \mathrm{symm}\, \boldsymbol{\sigma} \cdot \mathrm{symm}\, \nabla \boldsymbol{u} \mathrm{d}V - \Pi^{ext}(\boldsymbol{u}) \tag{11}$$

or it can be written explicitly in terms of lateral deflection and rotation fields

$$\Pi(w, \boldsymbol{\theta}) = \frac{1}{2} \int_{\Omega} \boldsymbol{\kappa}^T \boldsymbol{C}^b \boldsymbol{\kappa} \mathrm{d}A + \frac{1}{2} \int_{\Omega} \boldsymbol{\gamma}^T \boldsymbol{C}^s \boldsymbol{\gamma} \mathrm{d}A - \Pi^{ext}(\boldsymbol{u}) \tag{12}$$

The corresponding variational formulation is derived from the updated total energy functional of a body, which δw and $\delta \boldsymbol{\theta}$ represent variations of lateral displacement, rotation fields

$$G_{\boldsymbol{u}}(w, \boldsymbol{\theta}; \delta w, \delta \boldsymbol{\theta}) = \int_{\Omega} \delta \boldsymbol{\kappa}^T \boldsymbol{M} \mathrm{d}A + \int_{\Omega} \delta \boldsymbol{\gamma}^T \boldsymbol{Q} \mathrm{d}A - G^{ext}(w; \delta w) = 0 \tag{13}$$

where the external virtual work $G^{ext}(w; \delta w)$, in which δw is a variation of lateral displacement w, is formulated in the spirit of d'Alembert principle with an additional term from inertia force for elastodynamics problem

$$G^{ext}(w; \delta w) = \int_{\partial \Omega_2} \delta w q \mathrm{d}A - \int_{\Omega} \delta w \rho \ddot{w} \mathrm{d}V \tag{14}$$

This formulation, although simple as its derivation, is considered to be inefficient due to the locking behavior in the plate.

2.3 Two-field variational approach

Independent stress field
The variational formulation is based on a Hellinger-Reissner functional, where both displacement and stress are viewed as independent fields, see Gruttmann and Wagner (2004)

$$\Pi_{HR}(\mathbf{u}, \boldsymbol{\sigma}) = \int_{\Omega} \left(\boldsymbol{\epsilon}^T \boldsymbol{\sigma} - \frac{1}{2} \boldsymbol{\sigma}^T \mathbf{C}^{-1} \boldsymbol{\sigma} \right) dA - \int_{\Omega} \mathbf{u}^T \overline{\mathbf{p}} dA - \int_{\Gamma_{\sigma}} \mathbf{u}^T \overline{\mathbf{t}} ds \tag{15}$$

in which $\overline{\boldsymbol{p}}$ and $\overline{\boldsymbol{t}}$ are transverse and boundary loads. The corresponding variation equation with respect to displacement and stress fields are given as

$$\delta \Pi_{HR}(\mathbf{u}, \boldsymbol{\sigma}; \delta \mathbf{u}, \delta \boldsymbol{\sigma}) = \int_{(\Omega)} \left[\delta \boldsymbol{\epsilon}^T \boldsymbol{\sigma} + \delta \boldsymbol{\sigma}^T \left(\boldsymbol{\epsilon} - \mathbf{C}^{-1} \boldsymbol{\sigma} \right) - \delta \mathbf{u}^T \overline{\mathbf{p}} \right] dA - \int_{(\Gamma_{\sigma})} \delta \mathbf{u}^T \overline{\mathbf{t}} ds = 0 \tag{16}$$

Independent shear force field
In another approach, the shear force is introduced as additional independent field, see Auricchio and Taylor (1994)

$$\Pi(w, \boldsymbol{\theta}, \boldsymbol{S}) = \frac{1}{2} \int_A \left[\boldsymbol{K}^T(\boldsymbol{\theta}) \boldsymbol{D}_B \boldsymbol{K}(\boldsymbol{\theta}) \right] \mathrm{d}A - \frac{1}{2} \int_A \left[\boldsymbol{S}^T \boldsymbol{D}_S^{-1} \boldsymbol{S} \right] \mathrm{d}A$$
$$+ \int_A \left[\boldsymbol{S}^T (\nabla w + \boldsymbol{e}\boldsymbol{\theta}) \right] \mathrm{d}A + \Pi_{\mathrm{ext}} \tag{17}$$

Regularized variational principle

The two-field variational formulation with displacement and stress as independent fields can be referred to the work of Hughes and Brezzi (1989)

$$\Pi_\gamma(\boldsymbol{u}, \boldsymbol{\sigma}) = -\frac{1}{2} \int_\Omega \mathrm{symm}\, \boldsymbol{\sigma} \cdot \mathbb{C}^{-1} \mathrm{symm}\, \boldsymbol{\sigma} \mathrm{d}V + \int_\Omega \mathrm{symm}\, \boldsymbol{\sigma} \cdot \mathrm{symm}\, \nabla \boldsymbol{u} \mathrm{d}V$$
$$+ \frac{1}{2} \gamma^{-1} \int_\Omega |\, \mathrm{skew}\, \boldsymbol{\sigma}|^2 \mathrm{d}V - \Pi^{ext}(\boldsymbol{u}) \tag{18}$$

From the above regularize equation, we can write the corresponding regularized variational principle for plate problem with independent fields including lateral deflection, rotation and moment

$$\Pi_\gamma(w, \boldsymbol{\theta}, \boldsymbol{M}) = -\frac{1}{2} \int_\Omega \mathrm{symm}\, \boldsymbol{M}^T \boldsymbol{D}^b \mathrm{symm}\, \boldsymbol{M} \mathrm{d}A + \int_\Omega \mathrm{symm}\, \boldsymbol{M}^T \boldsymbol{\kappa} \mathrm{d}A$$
$$+ \frac{1}{2} \int_\Omega \boldsymbol{\gamma}^T \boldsymbol{C}^s \boldsymbol{\gamma} \mathrm{d}A + \frac{1}{2} \frac{12}{t^3} \gamma^{-1} \int_\Omega |\, \mathrm{skew}\, \boldsymbol{M}|^2 \mathrm{d}A - \Pi^{ext}(\boldsymbol{u}) \tag{19}$$

The corresponding variational formulation is derived from the updated total energy functional of a body, in which δw, $\delta\boldsymbol{\theta}$ and $\delta\mathbf{M}$ represent variations of lateral displacement, rotation and moment fields

$$G_{\boldsymbol{u}}(w, \boldsymbol{\theta}, \boldsymbol{M}; \delta w, \delta\boldsymbol{\theta}) = \int_\Omega \delta\boldsymbol{\kappa}^T \boldsymbol{M} \mathrm{d}A + \int_\Omega \delta\boldsymbol{\gamma}^T \boldsymbol{C}^s \boldsymbol{\gamma} \mathrm{d}A - G^{ext}(w; \delta w) = 0 \tag{20}$$

The variation formulation of regularized functional with respect to virtual moment $\delta\mathbf{M}$ can be written as follows

$$G_{\boldsymbol{M}}(\boldsymbol{\kappa}, \boldsymbol{M}; \delta\boldsymbol{M}) = \int_A \delta\boldsymbol{M}^T \left[\boldsymbol{\kappa} - \hat{\boldsymbol{D}}^b \boldsymbol{M} \right] \mathrm{d}A \tag{21}$$

In the same manner, the regularized formulation Eq. (18) can be reconfigured by adding independent shear field

$$\Pi_\gamma(w, \boldsymbol{\theta}, \boldsymbol{M}, \boldsymbol{Q}) = -\frac{1}{2} \int_A \left(\mathrm{symm}\, \boldsymbol{M}^T \boldsymbol{D}^b \mathrm{symm}\, \boldsymbol{M} + \boldsymbol{Q}^T D^s \boldsymbol{Q} \right) \mathrm{d}A$$
$$+ \int_A \left(\mathrm{symm}\, \boldsymbol{M}^T \boldsymbol{\kappa} + \boldsymbol{Q}^T \boldsymbol{\gamma} \right) \mathrm{d}A + \frac{1}{2} \bar{\gamma}^{-1} \int_A \frac{12}{t^3} |\, \mathrm{skew}\, \boldsymbol{M}|^2 \mathrm{d}A - \Pi^{ext}(\boldsymbol{u}) \tag{22}$$

The corresponding variational formulation with respect to variations of lateral deflection, rotation, moment and shear force fields can be written as follows

$$G_{\boldsymbol{u}}(w, \boldsymbol{\theta}, \boldsymbol{M}, \boldsymbol{Q}; \delta w, \delta\boldsymbol{\theta}) \quad = \int_A \delta\boldsymbol{\kappa}^T \boldsymbol{M} \mathrm{d}A + \int_A \delta\boldsymbol{\gamma}^T \boldsymbol{Q} \mathrm{d}A - G^{ext}(w; \delta w) = 0$$
$$G_{\boldsymbol{M}, \boldsymbol{Q}}(w, \boldsymbol{\theta}, \boldsymbol{M}, \boldsymbol{Q}; \delta\boldsymbol{M}, \delta\boldsymbol{Q}) \quad = \int_A \left[\delta\boldsymbol{M}^T \left(\boldsymbol{\kappa} - \hat{\boldsymbol{D}}^b \boldsymbol{M} \right) + \delta\boldsymbol{Q}^T \left(\boldsymbol{\gamma} - D^s \boldsymbol{Q} \right) \right] \mathrm{d}A = 0 \tag{23}$$

The above proposals can be promising with an appropriate discretization of moment and shear force fields, which is favorable for wave propagation prolems. Several other multi-field variational

approaches are successfully implemented, which are mentioned correspondingly in the next section. The same approach is successfully applied in axisymmetric and two-dimensional plane plate problems, see Nguyen and Ibrahimbegovic (2020) and Nguyen and Ibrahimbegovic (2020).

3. Notable highlights: simple and efficient locking-free approaches

Due to the numerous available developments of locking-free finite plate bending elements, we only choose several notable algorithms to present their corresponding key ideas and methods. The reader is highly recommended to refer to Zienkiewicz *et al.* (2005), Batoz and Dhatt (1990) and Batoz and Dhatt (1992) for the almost full set of relevant state-of-the-art algorithms.

3.1 Assumed shear strain

DKMT/DKMQ element

The so-called DKMT and DKMQ elements without spurious zero-energy modes are developed to pass the patch test for both thick finite plate element in an arbitrary mesh and is free of shear locking, see Katili (1993), Batoz and Katili (1992) and Katili *et al.* (2014). The variational functional of the modified Hu-Washizu principle is given as

$$\Pi = \Pi_{\mathrm{b}}\left(\beta_x, \beta_y\right) + \Pi_{\mathrm{s}}\left(w, \beta_x, \beta_y, \{\gamma\}, \{T\}\right) - \Pi_f\left(w, \beta_x, \beta_y\right) \tag{24}$$

in which the bending Π_{b} and shear strain Π_{s} energies are given as

$$\Pi_{\mathrm{b}} = \frac{1}{2}\int_{A^{\mathrm{e}}} \langle\chi\rangle\,[H_{\mathrm{b}}]\,\{\chi\}\mathrm{d}A$$

$$\Pi_{\mathrm{s}} = \frac{1}{2}\int_{A^{\mathrm{e}}} \langle\bar{\gamma}\rangle\,[H_{\mathrm{s}}]\,\{\bar{\gamma}\}\mathrm{d}A + \int_{A^{\mathrm{e}}} \langle\mathrm{T}\rangle(\{\gamma\} - \{\bar{\gamma}\})\mathrm{d}A \tag{25}$$

$$\Pi_{\mathrm{f}} = \int_A w f_z\ \mathrm{d}A + \int_{S_{\mathrm{r}}} (w F_z + \beta_x m_x + \beta_y m_y)\ \mathrm{d}s$$

The corresponding shear force, curvature, real shear strain and assumed shear strain matrices are given as follows

$$\langle T\rangle = \langle T_x\ \ T_y\rangle,\quad \langle\chi\rangle = \langle\chi_x\ \ \chi_y\ \ \chi_{xy}\ \rangle,\quad \langle\gamma\rangle = \langle\gamma_x\ \ \gamma_y\rangle,\quad \langle\bar{\gamma}\rangle = \langle\bar{\gamma}_x\ \ \bar{\gamma}_y\rangle \tag{26}$$

The $[H_{\mathrm{b}}]$ and $[H_{\mathrm{s}}]$ matrices depend on material properties, similar as Eq. (9). The stationary condition of variational functional Π in Eq. (25) with respect to the independent shear field yield

$$\int_{A^c} \langle\delta T\rangle(\{\gamma\} - \{\bar{\gamma}\})\mathrm{d}A = 0 \tag{27}$$

Hence, the real shear strain $\{\gamma\}$, expressed in terms of the element degree of freedom, is replaced by various discrete constraints on each element to relate the independent (or assumed) shear strains $\{\bar{\gamma}\}$, see Fig. 2. Correspondingly, this approach can avoid shear locking $\{\gamma\}$.

The displacement field is given as follows

$$u = z\beta_x(x, y),\quad v = z\beta_y(x, y),\quad w = w(x, y) \tag{28}$$

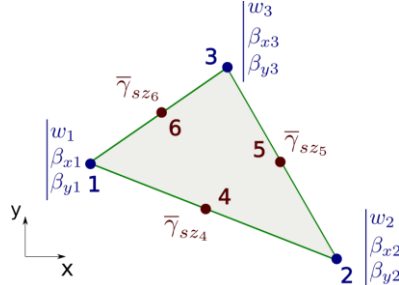The assumed tangential shear strain fields are given as follows
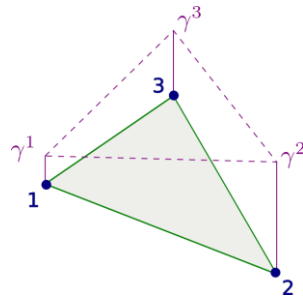
Fig. 2 Assumed tangential shear strain at mid-edges

Fig. 3 Assumed shear strain γ

$$\bar{\gamma}_{sz_k} = \frac{D_b}{D_s}\beta_{s,ss} = -\frac{2}{3}\phi_k\Delta\beta_{sk}, \quad \phi_k = \frac{2}{k(1-\nu)}\frac{h^2}{L_k^2} \tag{29}$$

where $k=5/6$ is the shear correction factor, v is Poisson's ratio, h is the thickness of the plate, L_k is the length of the side k and ϕ_k is the shear influence factor. $\Delta\beta_{sk}$ are the nodal values at the mid-nodes and s denotes the tangential direction. The tangential shear angles of sides k and m is further expressed in terms of the shear angle components γ_{xzi} and γ_{yzi} at corner node i. Finally, the transverse shear strain $\{\bar{\gamma}\}$ is interpolated independently with

$$\{\bar{\gamma}\} = \left\{ \begin{array}{c} \bar{\gamma}_{xz} \\ \bar{\gamma}_{yz} \end{array} \right\} = [N_\gamma]\{\bar{\gamma}_n\}, \quad \langle\bar{\gamma}_n\rangle = \langle\bar{\gamma}_{sz4} \ \bar{\gamma}_{sz5} \ \bar{\gamma}_{sz6}\rangle \tag{30}$$

A triangular element

To alleviate the shear locking, the nodal shear strains $\boldsymbol{\gamma}^i$, see Fig. 3, are computed in the manner that ensures the constant shear strain distribution along each edge, and thus continuity between adjacent plate element. By enforcing the equality between the projection of the nodal shear strain along the edge of two neighbors, see Ibrahimbegovic (1993), the corresponding matrix of nodal shear strain is formed as a function of nodal unknown matrix **d**.

The interpolation nodal parameters of shear strain are computed as follows. We consider a typical node i, with adjacent nodes j and k. The shear strain γ_{tij} along edge ij is constant and equal to

$$\gamma_{t_{ij}} = \frac{1}{l_{ij}}\left(w^j - w^i\right) - \frac{1}{2}\boldsymbol{n}_{ij}^T\left(\boldsymbol{\theta}^j + \boldsymbol{\theta}^i\right) \tag{31}$$

while the shear strain γ_{tik} along edge ik is the constant and equal to

$$\gamma_{t_{ik}} = \frac{1}{l_{ik}} \left(w^k - w^i \right) - \frac{1}{2} \boldsymbol{n}_{ik}^T \left(\boldsymbol{\theta}^k + \boldsymbol{\theta}^i \right) \tag{32}$$

in which the symbols l_{ij} and $\mathbf{n}_{ij}$ are, respectively, the length and the outward unit normal vector for the edge between the corner nodes i and j

$$l_{ij} = \left[(x_{j1} - x_{i1})^2 + (x_{j2} - x_{i2})^2 \right]^{1/2} \quad \boldsymbol{n}_{ij} = \frac{1}{l_{ij}} (x_{j2} - x_{i2}, x_{i1} - x_{j1}) \tag{33}$$

The projection of the nodal shear strain γ_i on the edges ij and ik is imposed to be equal, respectively, to γ_{tij} and γ_{tik}. The vectors $\mathbf{n}_{ik}$ and $\mathbf{t}_{ik}$ are normal and tangent vectors of edge ik

$$\boldsymbol{t}_{ij}^T \boldsymbol{\gamma}^i = \gamma_{t_{ij}} \Rightarrow \boldsymbol{n}_{ik} \boldsymbol{t}_{ij}^T \boldsymbol{\gamma}^i = \boldsymbol{n}_{ik} \gamma_{t_{ij}} \quad \boldsymbol{t}_{ik}^T \boldsymbol{\gamma}^i = \gamma_{t_{ik}} \Rightarrow \boldsymbol{n}_{ij} \boldsymbol{t}_{ik}^T \boldsymbol{\gamma}^i = \boldsymbol{n}_{ij} \gamma_{t_{ik}} \tag{34}$$

Hence

$$\boldsymbol{\gamma}^i = \underbrace{\frac{1}{\boldsymbol{n}_{ik} \boldsymbol{t}_{ij}^T - \boldsymbol{n}_{ij} \boldsymbol{t}_{ik}^T}}_{\Lambda^i} \left(\boldsymbol{n}_{ik} \gamma_{t_{ij}} - \boldsymbol{n}_{ij} \gamma_{t_{ik}} \right) \tag{35}$$

with indices are defined as

$$i = \{1, 2, 3\}; \quad j = (i, 3) + 1; \quad k = i - 1 + 3 \operatorname{int}(1/i) \tag{36}$$

The following identity holds $\Lambda^i = \frac{I}{t_{ij}^T n_{ik}}$ thanks to the symmetry property of $\lambda = n_{ik} t_{ij}^T - n_{ij} t_{ik}^T$ and orthogonal property between normal $\mathbf{n}_{ik}$ and tangent $\mathbf{t}_{ik}$ vectors on edge ik

$$\left. \begin{array}{l} \lambda n_{ik} = n_{ik} \lambda \\ \lambda n_{ik} = n_{ik} t_{ij}^T n_{ik} - n_{ij} \underbrace{t_{ik}^T n_{ik}}_{0} = n_{ik} t_{ij}^T n_{ik} \end{array} \right\} \Rightarrow n_{ik} \lambda = n_{ik} t_{ij}^T n_{ik} \Rightarrow \frac{I}{t_{ij}^T n_{ik}} = \lambda^{-1} \equiv \Lambda_i \tag{37}$$

3.2 Internal bubble modes

The lateral deflection, rotations and shear forces are interpolated independtly, see Auricchio and Taylor (1994). The rotational field is enriched by internal degrees of freedom and linked to the lateral deflection

$$w = \boldsymbol{N}_w w + \boldsymbol{N}_{w\theta} \theta, \quad \boldsymbol{\theta} = N_\theta \hat{\boldsymbol{\theta}} + N_b \hat{\boldsymbol{\theta}}_b, \quad \boldsymbol{S} = N_S \hat{\boldsymbol{S}} \tag{38}$$

in which $\hat{\boldsymbol{\theta}}$ and $\hat{\boldsymbol{S}}$ denote respectively the internal rotational degrees of freedom and the shear stress degrees of freedom.

$$\begin{bmatrix} \boldsymbol{0} & \boldsymbol{0} & \boldsymbol{0} & \boldsymbol{K}_{Sw}^T \\ \boldsymbol{0} & \boldsymbol{K}_{\theta\theta} & \boldsymbol{K}_{b\theta}^T & \boldsymbol{K}_{S\theta}^T \\ \boldsymbol{0} & \boldsymbol{K}_{b\theta} & \boldsymbol{K}_{bb} & \boldsymbol{K}_{bS} \\ \boldsymbol{K}_{Sw} & \boldsymbol{K}_{S\theta} & \boldsymbol{K}_{bS}^T & \boldsymbol{K}_{SS} \end{bmatrix} \begin{Bmatrix} \hat{\boldsymbol{w}} \\ \hat{\boldsymbol{\theta}} \\ \hat{\boldsymbol{\theta}}_b \\ \hat{\boldsymbol{S}} \end{Bmatrix} = \begin{Bmatrix} \boldsymbol{f}_w \\ \boldsymbol{f}_\theta \\ \boldsymbol{0} \\ \boldsymbol{0} \end{Bmatrix} \tag{39}$$

By eliminating the internal rotational degrees of freedom and then the shear parameters, the stiffness matrix is condensed and the remaining unknowns are the external degrees of freedom.

3.3 High-order rotation field

The curvature is defined in terms of rotation $\boldsymbol{\beta}$ field, see Batoz (1982)

$$\{\chi\} = \left\{ \begin{array}{c} \partial\beta_x/\partial x \\ \partial\beta_y/\partial y \\ \partial\beta_x/\partial y + \partial\beta_y/\partial x \end{array} \right\} \tag{40}$$

The formulation of the discrete Kirchhoff quadrilateral element is thus based on the following considerations:

1. Incomplete cubic polynomial for approximation of rotation field

$$\beta_x = \sum_{i=1}^{8} N_i \beta_{x_i} \quad \beta_y = \sum_{i=1}^{8} N_i \beta_{y_i} \tag{41}$$

2. The Kirchhoff assumptions are introduced
(a) at the corner nodes:

$$\left\{ \begin{array}{c} \beta_{x_i} + w_{,x_i} \\ \beta_{y_i} + w_{,y_i} \end{array} \right\} = \left\{ \begin{array}{c} 0 \\ 0 \end{array} \right\} \quad i = 1, 2, 3, 4 \tag{42}$$

(b) at the mid-nodes

$$\beta_{s_k} + w_{,s_k} = 0 \quad k = 5, 6, 7, 8 \tag{43}$$

where *s* represents the co-ordinate along the element boundary.

3. $w_{,sk}$ is the derivative of the transverse displacement *w* with respect to s at the mid-node *k*

$$w_{,s_k} = \frac{-3}{2l_{ij}}\left(w_i - w_j\right) - \frac{1}{4}\left(w_{,s_i} + w_{,s_j}\right) \tag{44}$$

4. β_{nk} varies linearly along the sides, i.e.

$$\beta_{n_k} = \frac{1}{2}\left(\beta_{n_i} + \beta_{n_j}\right) = -\frac{1}{2}\left(w_{,n_i} + w_{n_j}\right) \tag{45}$$

3.4 Stabilized quadrilateral element

The low-order bilinear polynomials are employed to interpolate the lateral displacement and rotations

$$w = \mathbf{N}^T \mathbf{w}, \quad \beta_x = \mathbf{N}^T \boldsymbol{\beta}_x, \quad \beta_y = \mathbf{N}^T \boldsymbol{\beta}_y \tag{46}$$

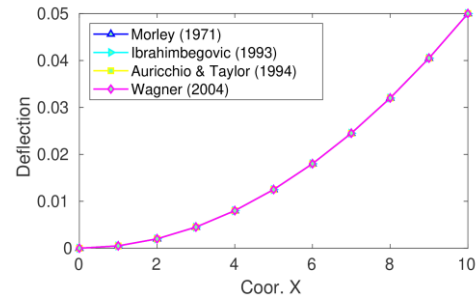Correspondingly, the stress field σ is also interpolated by linear functions, see Gruttmann and Wagner (2004)

$$\boldsymbol{\sigma}^h = \mathbf{S}\boldsymbol{\beta} \quad \mathbf{S} = \left[\mathbf{1}_{(5\times5)}, \overline{\mathbf{S}}\right] \quad \boldsymbol{\beta} = \left[\boldsymbol{\beta}^0, \boldsymbol{\beta}^1\right]^T$$

$$\tilde{\mathbf{S}} = \begin{bmatrix} J_{11}^0 J_{11}^0(\eta - \bar{\eta}) & J_{21}^0 J_{21}^0(\xi - \bar{\xi}) & 0 & 0 \\ J_{12}^0 J_{12}^0(\eta - \bar{\eta}) & J_{22}^0 J_{22}^0(\xi - \bar{\xi}) & 0 & 0 \\ J_{11}^0 J_{12}^0(\eta - \bar{\eta}) & J_{21}^0 J_{22}^0(\xi - \bar{\xi}) & 0 & 0 \\ 0 & 0 & J_{11}^0(\eta - \bar{\eta}) & J_{21}^0(\xi - \bar{\xi}) \\ 0 & 0 & J_{12}^0(\eta - \bar{\eta}) & J_{22}^0(\xi - \bar{\xi}) \end{bmatrix} \tag{47}$$

where the vectors $\boldsymbol{\beta}_0$ and $\boldsymbol{\beta}_1$ contain 5 and 4 parameters, respectively. The transformation coefficients
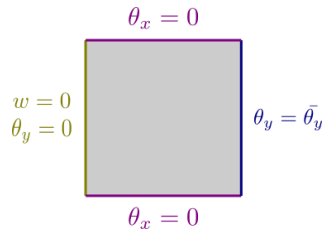
(a) Boundary condition   (b) Lateral deflection w

Fig. 4 Patch test

J^0 denote the components of the Jacobian matrix evaluated at the element center and transform the contravariant components of the stress resultant tensors to the Cartesian basis system. The coefficients have to be constant in order to fulfill the patch test.

4. Numerical simulations: Selective algorithms

In the following section, the efficient algorithms proposed by Ibrahimbegovic (1993) and Gruttmann and Wagner (2004) are programmed by FORTRAN language, which are integrated as user-defined subroutines in FEAP v8.4 program. Additionally, the algorithm for thin plate bending problem by Morley (1971) is also programmed for the comparison. The numerical results from above finite elements are illustrated together with Auricchio and Taylor (1994), which is a built-in subroutine inside FEAP.

4.1 Patch test

The patch test is delivered in pure bending along x direction. This test not only check the element performance but also reveal any spurious modes which may exist. The geometric properties of plate are: each side 10×10 and thickness $t= 0.1$. The imposed boundary conditions for the patch test are shown in Fig. 4(a). The regular mesh is constructed by 10×10 divisions, with total 200 triangular elements. The material parameters chosen in this simulation are: elastic modulus E=10.92 and Poisson's ratio v=0.3. The right edge is imposed by a rotation θ_y=−0.01 while the rotation θ_x at the top and bottom edges are set free. The left edge is fixed in three degrees of freedom. With this boundary configuration, the plate is bending upward as a simple beam in two-dimensional problem. It is clear that the lateral deflection w along the plate, see Fig. 4(b), is nearly equal within the four algorithms which includes the thick and thin finite elements. This is due to the rather small thickness of the plate. All elements pass the patch test with a constant curvature as ε_{xx}=−10^{-6}. The contours of lateral deflection w and rotation θ_y over entire domain by Auricchio and Taylor (1994) are shown in Fig. 5.

4.2 Simply supported circular plate

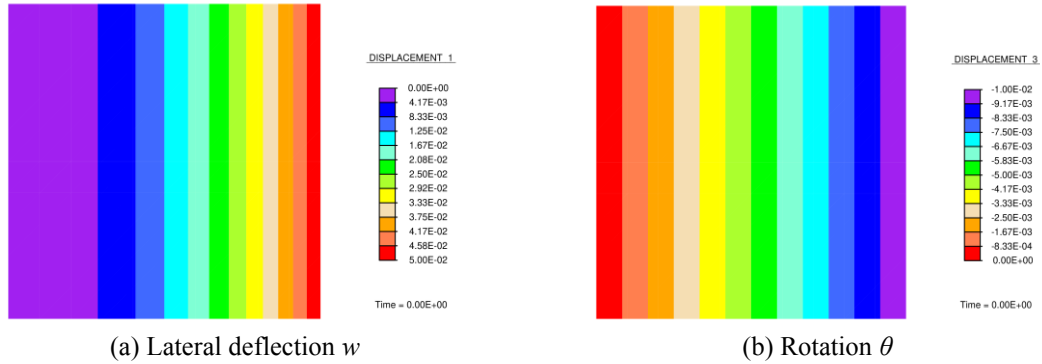A circular plate test is proposed to assess element's performance for a distorted mesh. The chosen

(a) Lateral deflection *w*

(b) Rotation *θ*

Fig. 5 Patch test: lateral deflection *w* and rotation θ_y fields
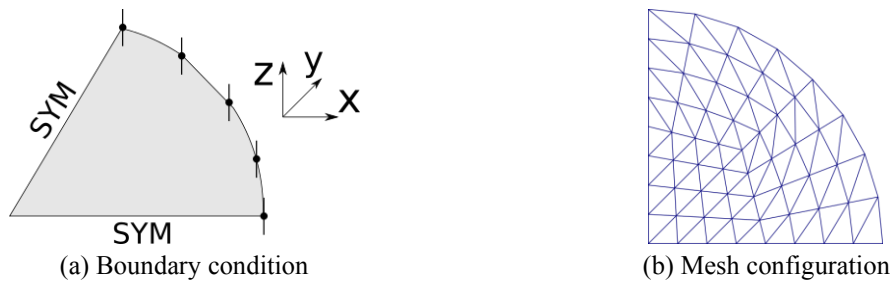

(a) Boundary condition

(b) Mesh configuration

Fig. 6 Circular plate boundary condition and mesh configuration

circular plate geometry is: radius *R*=5 and thickness *t*=1. The material properties are selected as: Young's modulus *E*=10.92 and Poisson's ratio *v*=0.3. The circular plate is imposed by a unit point load *P*=1 at the center and a surface loading *q*=1. The simply support boundary condition is considered. Only a quarter of the plate is used in this simulation with imposed symmetry boundary conditions on two radial lines, see Fig. 7(a). The subsequent finer meshes is generated by bisection of each three blocks used to construct the mesh with total 192 triangular elements, see Fig. 7(b). The exact solution of center deflection under surface load can be found at Batoz and Dhatt (1990) as follows

$$w_c = \frac{q \times R^4}{64 \times D} \left(\frac{\mu + 5}{\mu + 1} + \phi \right), \quad \phi = \frac{16}{5} \left(\frac{t}{R} \right)^2 \frac{1}{1 - \nu} \tag{41}$$

and the flexural rigidity D$= \dfrac{E \times h^3}{12 \left(1 - \nu^2\right)}$. Hence, the exact lateral deflection w_C is 41.6 under surface load.

Due to the significant thickness compared to the radius, the circular plate in this example is considered as the thick plate. The lateral deflection w is plotted along the radius as in Fig. 7(a) for the case of point load. Meanwhile, for the case of surface load, it is noted that the solution from Auricchio and Taylor (1994) yields 41.3, which is nearly equal the exact solution. In both case, the result from Morley (1971) is the lowest one. The robustness of other results can be improved by generate a finer mesh configuration. The corresponding contours of lateral deflection w and rotation θ_x by using the element of Ibrahimbegovic (1993) are shown in Fig. 8 for the case of point load and
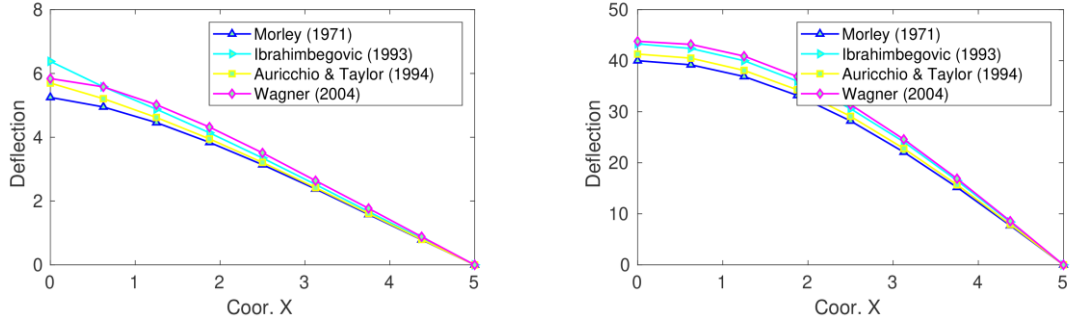
(a) Lateral deflection *w* under point load   (b) Lateral deflection *w* under surface load
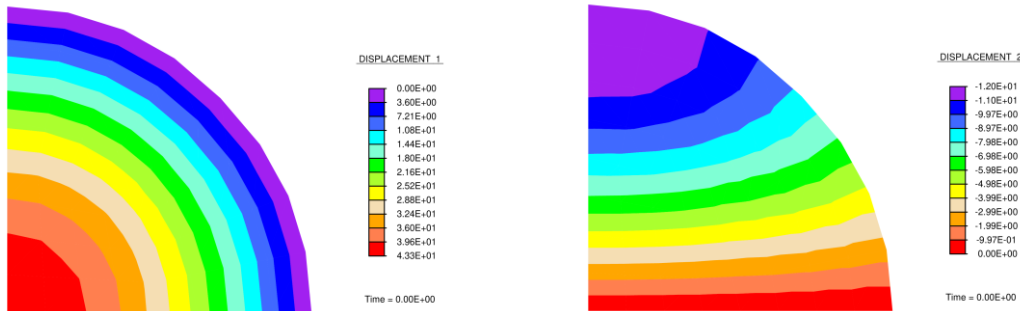
Fig. 7 Circular plate under point and surface loads
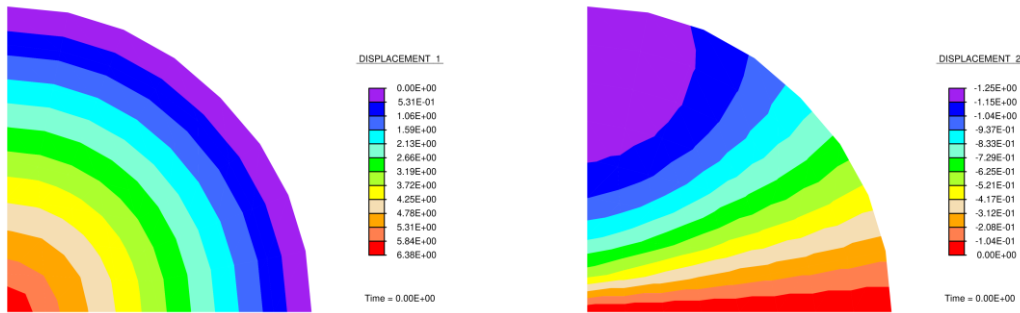
(a) Lateral deflection *w*   (b) Rotation θ_x

Fig. 8 Circular plate under point load: lateral displacement *w* and rotation θ_x fields

(a) Lateral deflection *w*   (b) Rotation θ_x

Fig. 9 Circular plate under surface load: lateral displacement *w* and rotation θ_x fields

Fig. 9 for the case of surface load. Due to the different load settings, the amplitude of contours are clearly discriminated. Meanwhile the trend of contours are quite similar.

4.3 Clamped square plate

In this example, we present the response of a square plate under point load *P*=1 applied at the center and and surface load *q*=1. The clamped boundary condition is imposed on outer edges. The
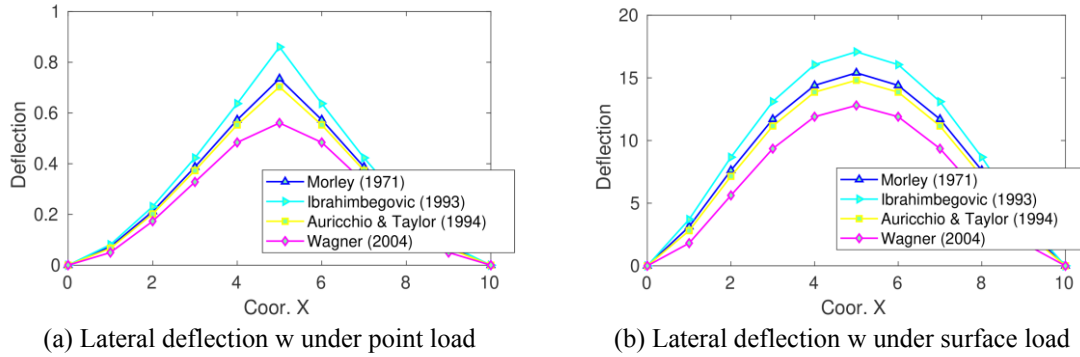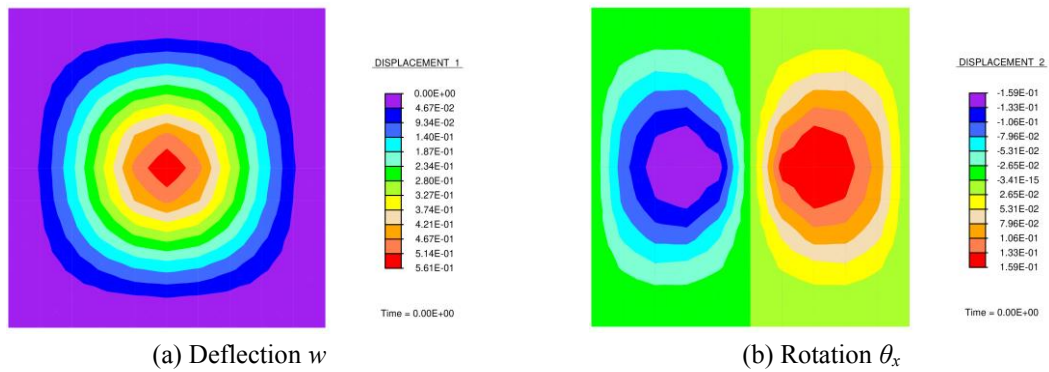
(a) Lateral deflection w under point load

(b) Lateral deflection w under surface load

Fig. 10 Square plate under point and surface loads

(a) Deflection *w*

(b) Rotation θ_x

Fig. 11 Square plate under point load: lateral displacement *w* and rotation θ_x fields
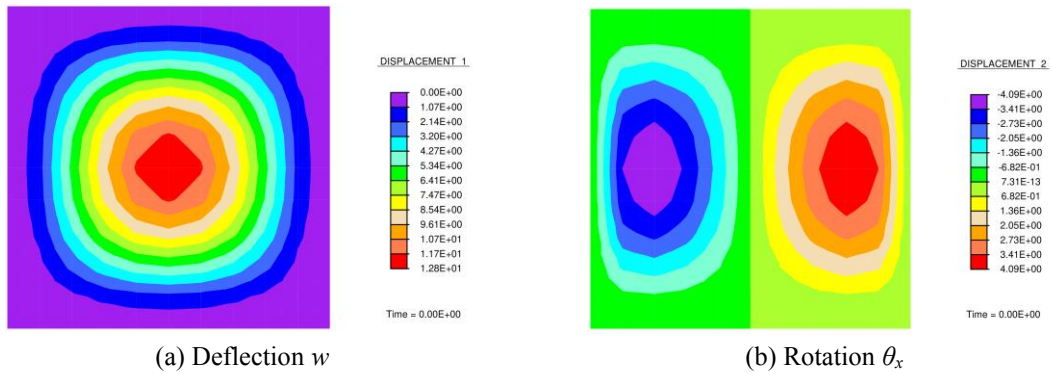

(a) Deflection *w*

(b) Rotation θ_x

Fig. 12 Square plate under surface load: lateral displacement *w* and rotation θ_x fields

plate is made of linear elastic isotropic material, with Young's modulus E=10.92 and Poisson's ratio v=0.3. The side length a=10 and thickness t=1 are selected. The numerical results are obtained by 10×10 regular mesh with total 200 triangular elements. The lateral deflection w is plotted along the horizontal line going through the square center.

In the current mesh configuration, the lateral deflection w from Morley (1971) and Auricchio and Taylor (1994) are comparable for both load cases, see Fig. 10. Meanwhile, the numerical solution

(a) Lateral deflection *w* under point load   (b) Lateral deflection *w* under surface load
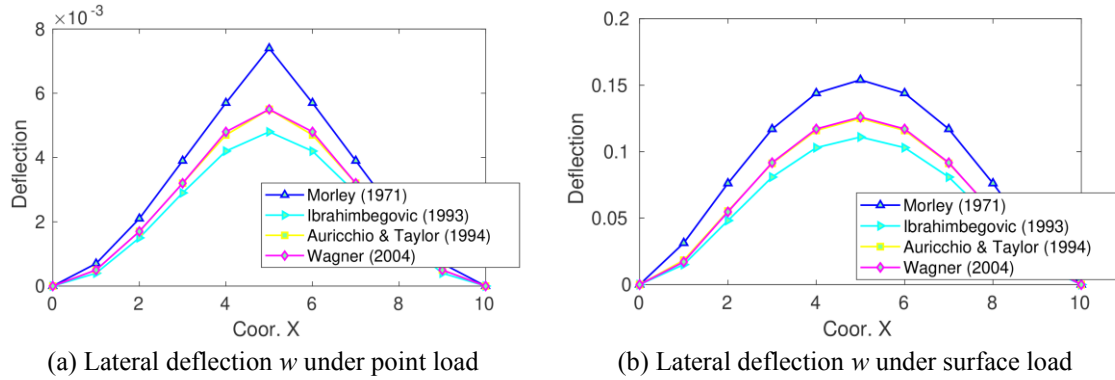
Fig. 13 Thin square plate under point and surface loads

from Morley (1971) seems to be higher than the other elements. By contrast, the result from Gruttmann and Wagner (2004) is lower or it tends to yield "stiffer" results than those from the other elements. The corresponding contours of lateral deflection w and rotation θ_x by Gruttmann and Wagner (2004) are shown in Fig. 11 for the case of point load and Fig. 12 for the case surface load. The contour distribution in both cases are similar.

In the following simulations, we use the same properties as previous one with the change of Young's modulus E=10.92×10^5 and thickness t=0.1, which can be viewed as a really thin plate. The numerical solutions from Auricchio and Taylor (1994) and Gruttmann and Wagner (2004) match together, see Fig. 13(a), (b). Meanwhile, the solution from Ibrahimbegovic (1993) is lower or "stiffer" than the others. It is clear that the solution from Morley (1971) is the highest one.

5. Conclusions

In this paper, we review briefly the highlights of selective locking-free algorithms for the Reissner-Mindlin plate bending problems. Firstly, theoretical background including fundamental concepts (derivation of stress and strain), one-field and two-field variational approaches are out-lined in a practical manner. Correspondingly, several simple and efficient techniques to overcome locking phenomenon in thick plate bending problems are presented and classified logically into a number of main categories. Finally, only selective finite elements among the illustrated algorithms are programmed by FORTRAN language in FEAP v8.4 program. The results from numerical simulations are compared between these elements and the built-in FEAP subroutine to present their robust performances.

Acknowledgments

References

Allaire, G. and Delgado, G. (2016), "Stacking sequence and shape optimization of laminated composite plates via a level-set method", *J. Mech. Phys. Solid.*, **97**, 168-196. https://doi.org/10.1016/j.jmps.2016.06.014.

Auricchio, F. and Taylor, R.L. (1994), "A shear deformable plate element with an exact thin limit", *Comput. Meth. Appl. Mech. Eng.*, **118**(3-4), 393-412. https://doi.org/10.1016/0045-7825(94)90009-4.

Auricchio, F. and Taylor, R.L. (1994), "A triangular thick plate finite element with an exact thin limit", *Finite Elem. Anal. Des.*, **19**(1-2), 57-68. https://doi.org/10.1016/0168-874X(94)00057-M.

Babuska, I. and Scapolla, T. (1989), "Benchmark computation and performance evaluation for a rhombic plate bending problem", *Int. J. Numer. Meth. Eng.*, **28**, 155-179. https://doi.org/10.1002/nme.1620280112.

Bathe, K.J. (2016), *Finite Element Procedures*, Prentice Hall, Pearson Education Inc, Massachusetts, USA.

Batoz, J.L. (1982), "An explicit formulation for an efficient triangular plate-bending element", *Int. J. Numer. Meth. Eng.*, **18**(7), 1077-1089. https://doi.org/10.1002/nme.1620180711.

Batoz, J.L. and Dhatt, G. (1990), *Modélisation des Structures par Elements Finis Vol. 2: Poutres et Plaques*, Herms, Paris, France.

Batoz, J.L. and Dhatt, G. (1992), *Modélisation des Structures par Elements Finis Vol. 3: Coques*, Herms, Paris, France.

Batoz, J.L. and Katili, I. (1992), "On a simple triangular reissner/mindlin plate element based on incompatible modes and discrete constraints", *Int. J. Numer. Meth. Eng.*, **35**(8), 1603-1632. https://doi.org/10.1002/nme.1620350805.

Batoz, J.L., Bathe, K.J. and Ho, L.W. (1980), "A study of three-node triangular plate bending elements", *Int. J. Numer. Meth. Eng.*, **15**, 1771-1812. https://doi.org/10.1002/nme.1620151205.

Bazeley, G.P., Cheung, Y.K., Irons, B.M. and Zienkiewicz, O.C. (1966), "Triangular elements in plate bending-Conforming and non-conforming solutions", Air Force Flight Dynamics Laboratory, 547-576.

Belblidia, F., Bae, J., Rechak, S. and Hinton, E. (2001), "Topology optimization of plate structures using a single- or three- layered artificial material model", *Adv. Eng. Softw.*, **32**(2), 159-168. https://doi.org/10.1016/S0045-7949(00)00141-3.

Brugnoli, A., Alazard, D., Valerie, P.B. and Matignon, D. (2019), "Port-Hamiltonian formulation and symplectic discretization of plate models Part I: Mindlin model for thick plates", *Appl. Math. Model.*, **75**, 940-60. https://doi.org/10.1016/j.apm.2019.04.035.

Brugnoli, A., Alazard, D., Valerie, P.B. and Matignon, D. (2019), "Port-Hamiltonian formulation and symplectic discretization of plate models Part II: Kirchhoff model for thin plates", *Appl. Math. Model.*, **75**, 961-981. https://doi.org/10.1016/j.apm.2019.04.036.

Cirak, F. and Ortiz, M. (2001), "Fully C[1] -conforming subdivision elements for finite deformation thin-shell analysis", *Int. J. Numer. Meth. Eng.*, **51**, 813-833. https://doi.org/10.1002/nme.182.

Clough, R.W. and Felippa, C.A. (1968), "A refined quadrilateral element for analysis of plate bending", Air Force Flight Dynamics Laboratory, USA.

Dolbow, J., Moes, N. and Belytschko, T. (2000), "Modeling fracture in MindlinReissner plates with the extended finite element method", *Int. J. Solid. Struct.*, **37**, 48-50. https://doi.org/10.1016/S0020-7683(00)00194-3.

Goo, S., Wang, S., Hyun, J. and Jung, J. (2016), "Topology optimization of thin plate structures with bending stress constraints", *Comput. Struct.*, **175**, 134-143. https://doi.org/10.1016/j.compstruc.2016.07.006.

Gruttmann, F. and Wagner, W. (2004), "A stabilized one-point integrated quadrilateral Reissner-Mindlin plate element", *Int. J. Numer. Meth. Eng.*, **61**, 2273-2295. https://doi.org/10.1002/nme.1148.

Guo, Y.Q., Batoz, J.L., Naceur, H., Bouabdallah, S., Mercier, F. and Barlet, O. (2000), "Recent developments on the analysis and optimum design of sheet metal forming parts using a simplified inverse approach", *Comput. Struct.*, **78**(1-3), 133-148. https://doi.org/10.1016/S0045-7949(00)00095-X.

Hrabok, M.M. and Hrudey, T.M. (1984), "A review and catalogue of plate bending finite elements", *Comput. Struct.*, **19**(3), 479-495. https://doi.org/10.1016/0045-7949(84)90055-5.

Huang, H.C. and Hinton. E. (1984), "A nine node Lagrangian Mindlin plate element with enhanced shear

interpolation", *Eng. Comput.*, **1**(4), 369-379. https://doi.org/10.1108/eb023593.

Hughes, T.J.R. and Brezzi, F. (1989), "On drilling degrees of freedom", *Comput. Meth. Appl. Mech. Eng.*, **72**(1), 105-121. https://doi.org/10.1016/0045-7825(89)90124-2.

Hughes, T.J.R. and Tezduyar, T. (1981), "Finite elements based upon mindlin plate theory with particular reference to the four-node bilinear isoparametric element", *J. Appl. Mech.*, **48**(3), 587-596. https://doi.org/10.1115/1.3157679.

Hughes, T.J.R., Taylor, R.L. and Kanoknukulchai, W. (1977), "A simple and efficient finite element for plate bending", *Int. J. Numer. Meth. Eng.*, **11**(10), 1529-1543. https://doi.org/10.1002/nme.1620111005.

Ibrahimbegovic, A. (1992), "Plate quadrilateral finite element with incompatible modes", *Commun. Appl. Numer. Meth.*, **8**, 497-504. https://doi.org/10.1002/cnm.1630080803.

Ibrahimbegovic, A. (1993), "Quadrilateral finite elements for analysis of thick and thin plates", *Comput. Meth. Appl. Mech. Eng.*, **110**, 195-209. https://doi.org/10.1016/0045-7825(93)90160-Y.

Ibrahimbegovic, A. (2009), *Nonlinear Solid Mechanics: Theoretical Formulations and Finite Element Solution Methods*, Springer, Berlin, Germany.

Katili, I. (1993), "A new discrete Kirchhoff-Mindlin element based on Mindlin-Reissner plate theory and assumed shear strain fields - Part I: An extended DKT element for thick plate bending analysis", *Int. J. Numer. Meth. Eng.*, **36**, 1859-1883. https://doi.org/10.1002/nme.1620361106.

Katili, I. (1993), "A new discrete Kirchhoff-Mindlin element based on Mindlin-Reissner plate theory and assumed shear strain fields - Part II: An extended DKQ element for thick plate bending analysis", *Int. J. Numer. Meth. Eng.*, **36**, 1885-1908. https://doi.org/10.1002/nme.1620361107.

Katili, I., Batoz, J.L., Maknun, I.J., Hamdouni, A. and Millet, O. (2014), "The development of DKMQ plate bending element for thick to thin shell analysis based on the Naghdi/Reissner/Mindlin shell theory", *Finite Elem. Anal. Des.*, **100**, 12-27. https://doi.org/10.1016/j.finel.2015.02.005.

Kiendl, J., Ambati, M., Lorenzis, L.D, Gomez, H. and Reali, A. (2016), "Phase-field description of brittle fracture in plates and shells", *Comput. Meth. Appl. Mech. Eng.*, **312**, 374-394. https://doi.org/10.1016/j.cma.2016.09.011.

Konno, J. and Stenberg, R. (2010), "Finite element analysis of composite plates with an application to the paper cockling problem", *Finite Elem. Anal. Des.*, **46**(3), 265-272. https://doi.org/10.1016/j.finel.2009.10.001.

Lavrencic, M. and Brank, B. (2021), "Hybrid-mixed low-order finite elements for geometrically exact shell models: Overview and comparison", *Arch. Comput. Meth. Eng.*, 1-35. https://doi.org/10.1007/s11831-021-09537-2.

Macchelli, A., Melchiorri, C. and Bassi, L. (2005), "Port-based modelling and control of the Mindlin plate", *Proceedings of the 44th IEEE Conference on Decision and Control*, Seville, Spain.

Mindlin, R. (1951), "Influence of rotatory inertia and shear on flexural motions of isotropic, elastic plates", *J. Appl. Mech.*, **38**, 18-31. https://doi.org/10.1115/1.4010217.

Moleiro, F., Mota Soares, C.M., Mota Soares, C.A. and Reddy, J.N. (2009), "Mixed least-squares finite element models for static and free vibration analysis of laminated composite plates", *Comput. Meth. Appl. Mech. Eng.*, **198**(21-26), 1848-1856. https://doi.org/10.1016/j.cma.2008.12.023.

Morley, L.S.D. (1971), "The constant-moment plate-bending element", *J. Strain Anal. Eng. Des.*, **6**(1), 6-20. https://doi.org/10.1243/03093247V061020.

Nguyen, C.U. and Ibrahimbegovic, A. (2020), "Hybrid-stress triangular finite element with enhanced performance for statics and dynamics", *Comput. Meth. Appl. Mech. Eng.*, **372**, 113381. https://doi.org/10.1016/j.cma.2020.113381.

Nguyen, C.U. and Ibrahimbegovic, A. (2020), "Visco-plasticity stress-based solid dynamics formulation and time-stepping algorithms for stiff case", *Int. J. Solid. Struct.*, **196-197**, 154-170. https://doi.org/10.1016/j.ijsolstr.2020.04.018.

Ortiz, M. and Morris, G.R. (1988), "C^0 finite element discretization of Kirchhoff's equations of thin plate bending", *Int. J. Numer. Meth. Eng.*, **26**, 1551-1566. https://doi.org/10.1002/nme.1620260707.

Reissner, E. (1945), "The effect of transverse shear deformation on the bending of elastic plates", *J. Appl. Mech.*, **12**, A69-A77. https://doi.org/10.1115/1.4009435.

Reissner, E. (1976), "On the theory of transverse bending of elastic plates", *Int. J. Solid. Struct.*, **12**(8), 545-554. https://doi.org/10.1016/0020-7683(76)90001-9.

Robinson, J. and Haggenmacher, G.W. (1979), "LORA-An accurate four node stress plate bending element", *Int. J. Numer. Meth. Eng.*, **14**(2), 296-306. https://doi.org/10.1002/nme.1620140214.

Schollhammer, D. and Fries. T.P. (2019), "Kirchhoff-Love shell theory based on tangential differential calculus", *Comput. Mech.*, **64**, 113-131. https://doi.org/10.1007/s00466-018-1659-5.

Taylor, R.L. (2014), "FEAP-A finite element analysis program", University of California, Berkeley.

Tessler, A. and Hughes, T.J.R. (1983), "An improved treatment of transverse shear in the Mindlin-Type four-node quadrilateral element", *Comput. Meth. Appl. Mech. Eng.*, **39**, 311-335. https://doi.org/10.1016/0045-7825(83)90096-8.

Ulmer, H., Hofacker, M. and Miehe, C. (2012), "Phase field modeling of fracture in plates and shells", *Proc. Appl. Math. Mech.*, **12**, 171-172. https://doi.org/10.1002/pamm.201210076.

Viebahn, N., Pimenta, P.M. and Schroder, J. (2017), "A simple triangular finite element for nonlinear thin shells: statics, dynamics and anisotropy", *Comput. Mech.*, **59**, 281-297. https://doi.org/10.1007/s00466-016-1343-6.

Zienkiewicz, O.C., Taylor, R.L. and Zhu, J.Z. (2005), *The Finite Element Nethod: Its Basis and Fundamentals*, Prentice Hall, Pearson Education Inc, USA.